

# Design of Nano Catalysts with Hierarchical Structure for C1 Chemistry (C1 化学用多階層ナノ触媒の設計)

## 1. 課題設定 (Introduction)

In recent years, due to the increasing energy demand, the process for C1 chemistry always keeps receiving growing attention, which can synthesize useful chemical products and fuel production derived from simple molecules such as HCN, CH<sub>4</sub>, CO<sub>2</sub>, CO/H<sub>2</sub> and CH<sub>3</sub>OH. Moreover, the catalyst always plays an important role in this catalytic reaction system for C1 chemistry. So, it is very necessary to design the hierarchical structure for the catalysts to improve the selectivities of the target products.

In this thesis, we synthesized different kinds of catalysts with hierarchical structure, and various reaction systems were applied to test their catalytic activity, that is, the bimodal pore catalysts for enhanced CO<sub>2</sub> methanation, the composite catalysts for synthesis of middle isoparaffin from syngas via FTS reaction.

## 2. 方法論 (Experimental Section)

### 2.1 Nanoparticles promoted Ni-based bimodal pore catalysts

The nanoparticles promoted bimodal pore catalysts were prepared by incipient-wetness impregnation method using nanoparticles modified bimodal pore silica as the supports and nickel nitrate aqueous solution as the impregnant. After the impregnation, the samples were dried in air at 120 °C for 12 h, and then calcined in air at 450 °C for 4 h to obtain the catalysts. The content of Ni in the catalysts was fixed at 20 wt.%. SiO<sub>2</sub>, Al<sub>2</sub>O<sub>3</sub>, and ZrO<sub>2</sub> nanoparticles modified bimodal pore catalysts were denoted as 20Ni/SiO<sub>2</sub>-Si, 20Ni/SiO<sub>2</sub>-Al and 20Ni/SiO<sub>2</sub>-Zr, respectively. For comparison, a conventional catalyst was also prepared by the impregnation of 20 wt.% Ni over the pristine SiO<sub>2</sub> support, which was named as 20Ni/SiO<sub>2</sub>.

### 2.2 Effective H-USY zeolite supported nano-cobalt bifunctional catalysts

The ultra-stable Y (USY) zeolite supported cobalt catalyst was prepared by the self-made polygonal physical sputtering method. Commercial H-USY powders (Tosoh Co., SiO<sub>2</sub>/Al<sub>2</sub>O<sub>3</sub>=6.3 molar ratio, 466 m<sup>2</sup>/g) were pre-calcined in air followed by cooling down to

room temperature. Metallic cobalt plate (purity 99.9%) was used as the sputtering target. 5.0 g of the pretreated zeolite powders was loaded into the cavity barrel. After that, the vacuum chamber was evacuated to  $8.0 \times 10^{-4}$  Pa, followed by introducing a pure Ar (purity: 99.995%) with a flow rate of  $29 \text{ mL min}^{-1}$  into the chamber until the pressure reached 2.0 Pa. The input power was controlled to 350 W. After 200 min sputtering, about 7 wt% of Co loaded onto the zeolite powder was obtained. Thereafter, a 1.0%  $\text{O}_2/\text{N}_2$  flow was gradually introduced into the cavity barrel to reach common pressure, and kept for 1 h to stabilize the metallic Co supported catalyst, denoted as Co/USY-S. The obtained catalyst was reduced in  $\text{H}_2$  at  $260^\circ\text{C}$  for 1h, denoted as Co/USY-S-260.

### *2.3 Hierarchical HZSM-5 zeolite with combined micropores and mesopores*

The hierarchical HZSM-5 zeolite was prepared by a mixed aqueous solution of aluminium isopropoxide, pluronic F127 (Sigma, MW=12600), tetraethylorthosilicate (TEOS) and distilled water under continuous stirring to get a clear solution. Then, tetrapropylammonium hydroxide (TPAOH) was added drop wise to the solution, and continued stirring at  $40^\circ\text{C}$  to form a gel. The molar ratio of the resultant gel was  $0.5 \text{ Al}_2\text{O}_3: 50 \text{ SiO}_2: 0.6 \text{ F127}: 6 \text{ TPAOH}: 2400 \text{ H}_2\text{O}$ . The gel was aged at  $60^\circ\text{C}$ , and dried at  $90^\circ\text{C}$  overnight. Finally, the solid gel was transferred to Teflon-lined reactor and crystallized by steam-assisted crystallization (SAC) method at  $160^\circ\text{C}$  for 18 h. The product was washed, dried and calcined at  $550^\circ\text{C}$  for 5 h. The hierarchical HZSM-5 zeolite was denoted as meso-HZSM-5. A conventional HZSM-5 zeolite (conv-HZSM-5), as a reference catalyst, was also prepared by the same method but without F127 addition.

### *2.4 Catalytic Evaluation*

Carbon dioxide methanation was conducted in a fixed-bed reactor (i.d. 9 mm, length 300 mm) at atmosphere pressure. The feeds and products were analyzed by on-line gas chromatograph (Shimadzu GC-8A) equipped with a Porapak Q column and a thermal conductivity detector (TCD). FTS tests were performed with a continuous flowing fixed-bed reactor from syngas. Gas products ( $\text{C}_1\text{-C}_6$ ) were analyzed by two on-line gas chromatographs. An ice trap of n-octane as solvent was equipped to capture heavy hydrocarbons in the effluent.

### 3. 実験・解析(Results and Discussion)

#### 3.1 CO<sub>2</sub> methanation

As seen from Fig. 1, the pristine SiO<sub>2</sub> exhibited unimodal pore size distribution centered at about 50 nm. After the modification of nanoparticles, bimodal pore structures were observed. Meanwhile, the large pore size slightly decreased from about 50 to 45 nm in bimodal pore structure. The small pores below 20 nm were formed by the self-organization of nanoparticles inside the large pores of SiO<sub>2</sub>. The increase of surface area and formation of bimodal pore structure by the nanoparticle modification would improve the dispersion of Ni.

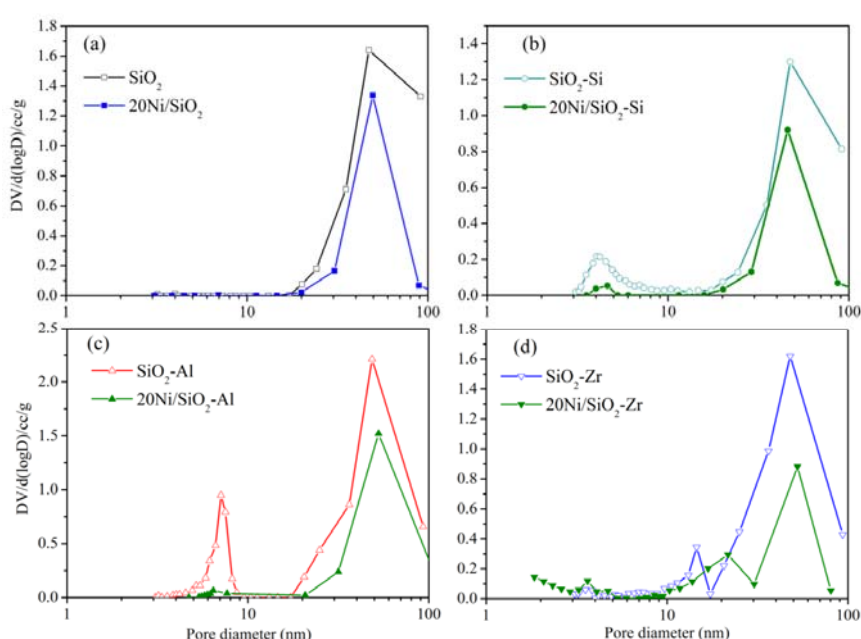


**Fig. 1** Pore size distributions of the pristine (a) and nanoparticle modified supports (b, c, d) and catalysts.

The pore structure parameters of the supports and catalysts are shown in Table 1. The pristine SiO<sub>2</sub> had a large pore size of 50 nm and small surface area of 70 cm<sup>2</sup>/g. After the modification of nanoparticles, the surface areas of the supports were improved significantly. The increase of surface areas was attributed to deposition of nanoparticles in the pores of the SiO<sub>2</sub>, which formed new porosity and extra surface area. Among these samples, ZrO<sub>2</sub> nanoparticles promoted SiO<sub>2</sub> exhibited the largest surface area while SiO<sub>2</sub> nanoparticles promoted support had the smallest surface area. The different improvement in surface area was probably due to the different diameters of the nanoparticles (Table 1) or the physico-chemical property of each nanoparticles sol.

**Table 1** Pore parameters of the supports and catalysts

Samples	BET area (m <sup>2</sup> /g)	Pore diameter (nm)	Pore volume (ml/g)
SiO <sub>2</sub>	70	50	1.10
SiO <sub>2</sub> -Si	97	4, 45	0.60
SiO <sub>2</sub> -Al	129	7, 45	0.75
SiO <sub>2</sub> -Zr	212	14, 45	0.64
20Ni/SiO <sub>2</sub>	61	50	0.62
20Ni/SiO <sub>2</sub> -Si	66	5, 45	0.47
20Ni/SiO <sub>2</sub> -Al	77	6, 52	0.76
20Ni/SiO <sub>2</sub> -Zr	135	20, 52	0.54

CO<sub>2</sub>-TPD was employed to evaluate the CO<sub>2</sub> adsorption and activation capability of the catalysts with different nanoparticles modification, and the results are compared in Fig. 2. The conventional catalyst 20Ni/SiO<sub>2</sub> exhibited one desorption peak at 181 °C, which was primarily attributed to the weakly adsorbed CO<sub>2</sub>. For the SiO<sub>2</sub> nanoparticles promoted catalyst, the peak for the weakly adsorbed CO<sub>2</sub> shifted to 202 °C, and a new peak at 505 °C appeared. The high temperature peak could be assigned to chemical sorption of CO<sub>2</sub> [1]. The introduction of SiO<sub>2</sub> nanoparticles enhanced the chemisorption of CO<sub>2</sub> and might improve the activity and selectivity for CO<sub>2</sub> methanation. For ZrO<sub>2</sub> and Al<sub>2</sub>O<sub>3</sub> nanoparticles modified catalysts, three desorption peaks centered at about 160, 300 and 400 °C were detected. The first peak at about 160 °C was due to the weakly adsorbed CO<sub>2</sub>, while the peaks at 300 and 400 °C might be related to the chemisorption and activation of CO<sub>2</sub> at different type of active centers [1]. It is clear that the area of peaks for chemical adsorbed CO<sub>2</sub> in 20Ni/SiO<sub>2</sub>-Zr was higher than that in 20Ni/SiO<sub>2</sub>-Al, which indicated a higher CO<sub>2</sub> methanation activity in 20Ni/SiO<sub>2</sub>-Zr catalyst.

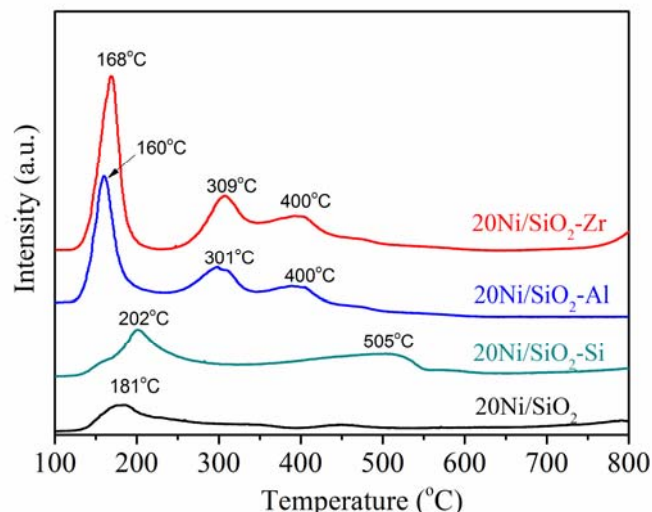


**Fig. 2** CO<sub>2</sub>-TPD profiles of the catalyst with different nanoparticles modification

Activity curves of the conventional and nanoparticles promoted bimodal pore catalysts for CO<sub>2</sub> methanation at different reaction temperature are shown in Fig. 3. For all the catalysts, the CO<sub>2</sub> conversion first increased, reached the maximum at 400 °C and then decreased with the increase of reaction temperature. The dependences of CH<sub>4</sub> selectivity on reaction temperatures are shown in Fig. 3b. For conventional and SiO<sub>2</sub> nanoparticles promoted catalysts, the methane selectivity first increased and then decreased with increasing the reaction temperature. It is interesting to find that there was a same variation trend for the CH<sub>4</sub> selectivity and CO<sub>2</sub> conversion with increasing the reaction temperature in 20Ni/SiO<sub>2</sub> and 20Ni/SiO<sub>2</sub>-Si catalysts. In other words, a higher CO<sub>2</sub> conversion is corresponding to a higher CH<sub>4</sub> selectivity. This can be interpreted by the sequence reaction mechanism of CO<sub>2</sub> methanation, where the first reaction involved the conversion of CO<sub>2</sub> to CO by reversed water gas shift reaction and then CO reacted with H<sub>2</sub> to form CH<sub>4</sub> [2, 3]. For ZrO<sub>2</sub> and Al<sub>2</sub>O<sub>3</sub> nanoparticles promoted catalysts, it is noted that the CH<sub>4</sub> selectivity was almost maintained at about 100 % until the reaction temperature increased to 450 °C, which is absolutely different from those of 20Ni/SiO<sub>2</sub> and 20Ni/SiO<sub>2</sub>-Si catalysts. The high CH<sub>4</sub> selectivity at low temperature for 20Ni/SiO<sub>2</sub>-Al and 20Ni/SiO<sub>2</sub>-Zr catalysts might be attributed to the high CO<sub>2</sub> chemisorption and activation capability as testified by the CO<sub>2</sub>-TPD.

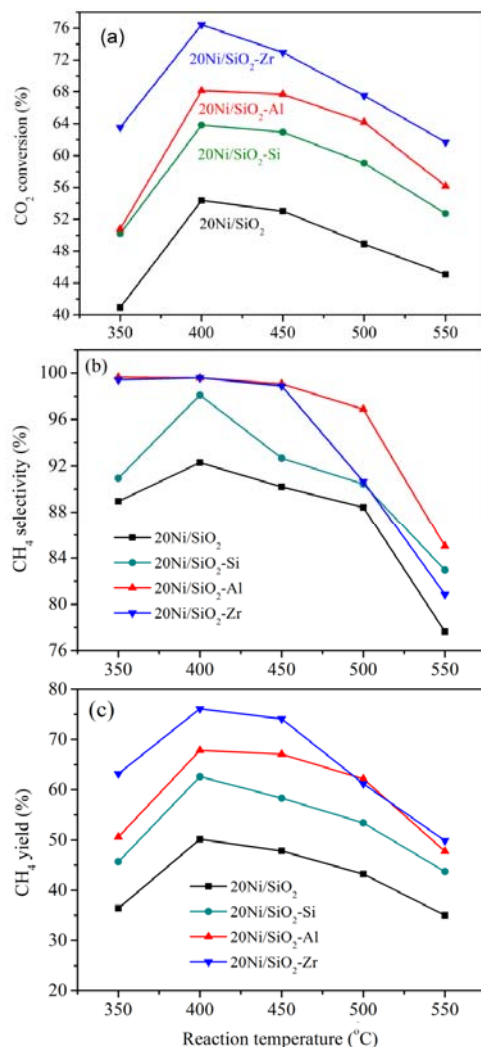


**Fig. 3** Catalytic activities of different nanoparticles modified catalysts: (a) CO<sub>2</sub> conversion, (b) CH<sub>4</sub> selectivity and (c) CH<sub>4</sub> yield. Reaction conditions: GHSV: 10,000 ml/(gh), CO<sub>2</sub>/H<sub>2</sub>=1:4, atmospheric pressure.

### 3.2 Sputtered catalysts for Selectively Converting Syngas to Gasoline

The particle size comparison of Co/USY-I and Co/USY-S was demonstrated in HRTEM images of Fig. 4. The impregnated Co particles exhibited large aggregation on USY zeolite with an average particle size of about 20 nm. But in the case of sputtered catalyst, cobalt nanoparticles were well-dispersed on zeolite with an average diameter of about 5 nm. Smaller and narrower particle distribution on the sputtered catalyst was attributed to the stir assistance of mechanical apparatus during the atomic-scale sputtering process [4, 5]. In detail, cobalt atoms derived from the attack by Ar plasma stream are homogenously deposited onto the USY zeolite surface with continuous hexagonal rotation and spin, as well as mechanical vibration provided by the rolling barrel. From H<sub>2</sub> chemisorption, a high Co dispersion of

17.2% was also observed for the sputtered Co/USY-S, much higher than that of 5.3% for the impregnated one. Herein, the higher cobalt dispersion on sputtered Co/USY-S catalyst contributed to better spatial arrangement of two kinds of active sites, making a more suitable and shorter distance between FTS sites and acidic sites nearby, if compared to the conventional impregnated one.

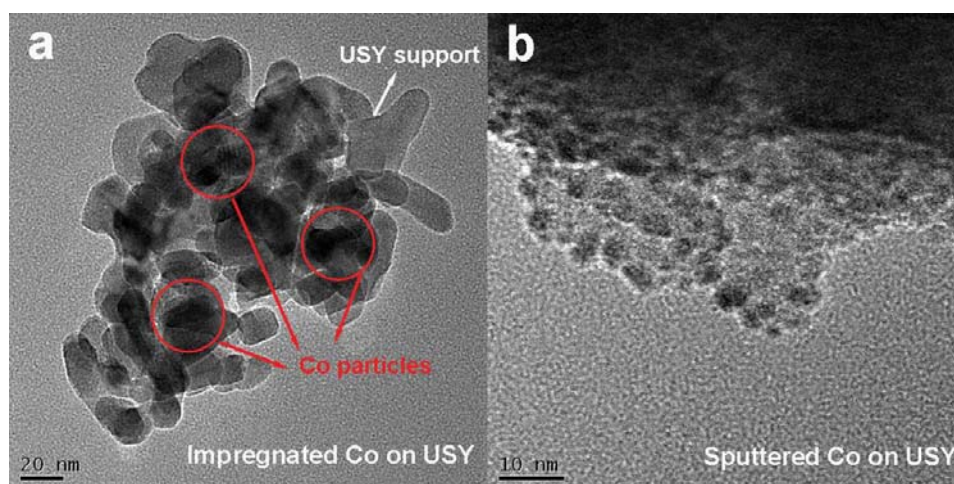


**Fig. 4** HRTEM images of the Co/USY-I (a) and Co/USY-S (b).

To demonstrate the chemical state of cobalt in different catalysts, surface analysis of the cobalt species was performed by XPS measurement. For the Co 2p spectra (Fig. 5), the binding energy peaks located at around 781 and 778 eV were generally attributed to the  $\text{Co}^{2+}$  and metallic Co (0) species, respectively [6]. The satellite peak at 786 eV further confirmed the existence of  $\text{Co}^{2+}$  species in all catalysts. The presence of the cobalt oxides for these catalysts was due to the stabilization treatment in 1%  $\text{O}_2$  after  $\text{H}_2$  reduction.

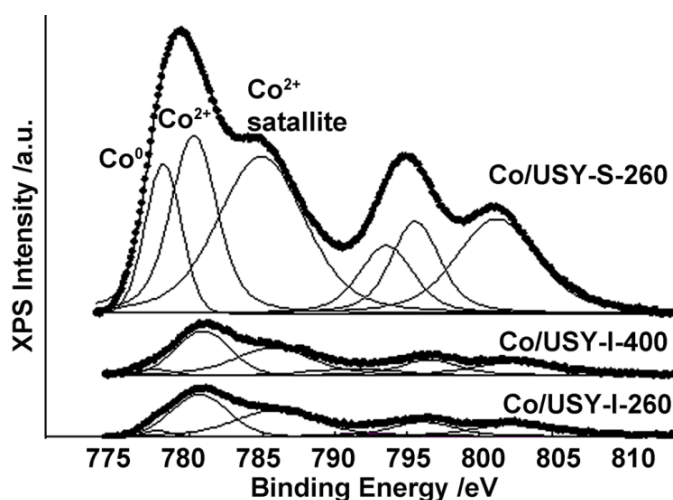


**Fig. 5** Co 2p XPS spectra of the reduced Co/USY-I and Co/USY-S catalyst.

Light and heavy hydrocarbon products were distributed differently on the two catalysts (Fig. 6). For the Co/USY-I-260, the main products were light hydrocarbons, including CH<sub>4</sub> and C<sub>2</sub>-C<sub>5</sub>. But for the case of sputtered one, hydrocarbons from C<sub>1</sub> to C<sub>4</sub> were decreased, and more C<sub>5</sub>-C<sub>11</sub> gasoline-ranged isoparaffins were derived. Herein, higher CH<sub>4</sub> selectivity on Co/USY-I was attributed to more unreduced cobalt oxides on zeolite.

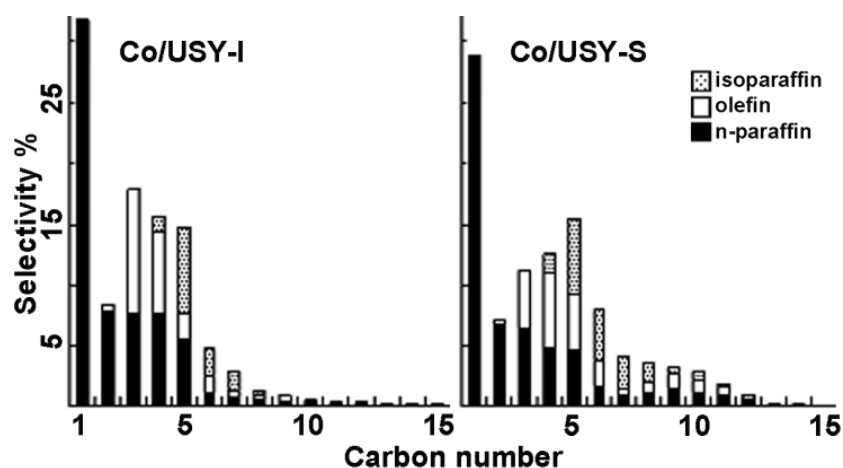


**Fig. 6** Hydrocarbon distribution on the Co/USY-I and Co/USY-S catalysts under iso-conversion FTS conditions.

### 3.3 Hierarchical HZSM-5 zeolite for FTS performance

Fig.7 shows the nitrogen adsorption and desorption isotherms of conv-HZSM-5 and meso-HZSM-5 samples. The conv-HZSM-5 exhibits type-I isotherm, a typical characteristic of microporous material. For comparison, the isotherm of meso-HZSM-5 sample reveals a type-IV isotherm. It contains a hysteresis loop at relative pressure higher than  $P/P_0=0.4$ , indicating the existence of mesopores. The pore size distribution of conv-HZSM-5 and meso-HZSM-5 obtained by using BJH method is displayed in Fig. 7b. For meso-HZSM-5 sample, an obvious mesopore size appears at 23.7 nm. These findings suggest that mesoporous HZSM-5 zeolite was one-step synthesized successfully as designed with the combination of micro-template (TPAOH) and meso-template (F127) as dual templates.



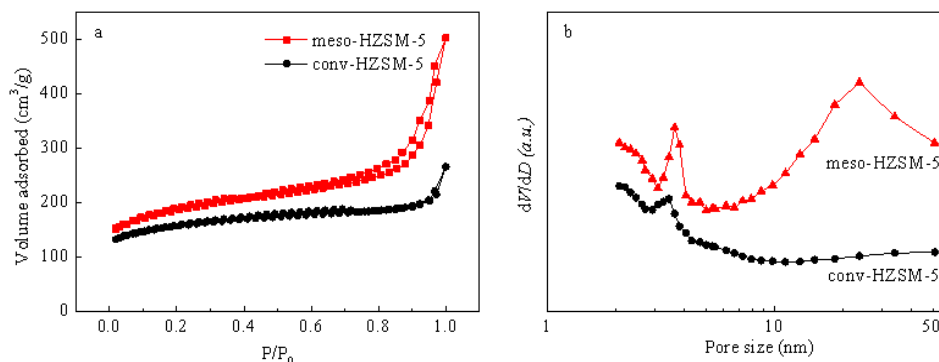


**Fig. 7** N<sub>2</sub> sorption isotherms and pore size distribution of the conv-HZSM-5 and meso-HZSM-5

The SEM and TEM images of the calcined meso-HZSM-5 are displayed in Fig. 8. The SEM image presents uniform spherical shape with a size around 500 nm. In addition, TEM image (Fig. 8b) shows the mesopores of 10-20 nm with combined micropores, indicating the presence of hierarchical pore structure, which will show an important effect on promoting the diffusion behavior of the reactants and the products.

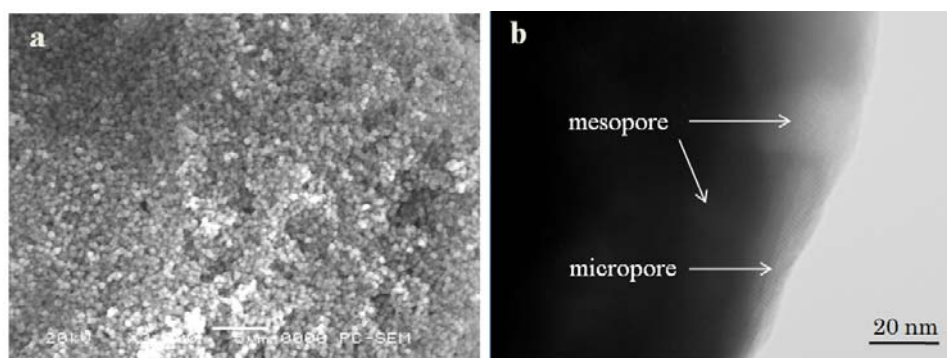


**Fig. 8** SEM (a) and TEM (b) images of the obtained meso-HZSM-5.

FTS performances and product distribution over different catalysts are presented in Table 2 and Fig. 9. The conventional HZSM-5 supported Co catalyst (Co/conv-HZSM-5) exhibits 75.9 % CO conversion and a wide FTS product distribution with C<sub>1-22</sub>. Contrarily, Co/meso-HZSM-5, the hierarchical HZSM-5 supported cobalt catalyst, gives higher CO conversion (79.0 %) and a narrow product distribution ranging from C<sub>1-18</sub> with lower 13.4 % CH<sub>4</sub> selectivity. At the same time, its selectivities of isoparaffin and C<sub>5+</sub> hydrocarbons are increased significantly. Furthermore, the gasoline components (C<sub>5-11</sub>) selectivity of 65.4 % is also increased if compared to that of the conventional catalyst (56.6 %). These findings are due to an enhancement in the diffusion efficiency of hydrocarbons and syngas inside the

mesoporous zeolite channels. The secondary reactions, including hydrocracking and isomerization of the primary hydrocarbons, proceed more quickly over acid sites at mesoporous channels in the hierarchical zeolite. Moreover, the C<sub>18+</sub> hydrocarbons are totally suppressed on Co/meso-HZSM-5 catalyst, accompanied by a sharp anti-ASF law product distribution. These results suggest that the increased pore size of support tunes the hydrocarbon distribution successfully, changing the selectivities of isoparaffin and olefin..

**Table 2** Tuned the FTS performance of different catalysts<sup>a</sup>

Catalyst	Conv. (%)	Product selectivity (%)							
		CO	CH <sub>4</sub>	CO <sub>2</sub>	n-paraffin	olefin	isoparaffin	C <sub>5-11</sub>	C <sub>5+</sub>
Co/conv-HZSM-5	75.9	14.8	1.7	52.8	30.9	16.2	56.6	70.7	0.50
Co/meso-HZSM-5	79.0	13.4	2.3	47.0	29.1	23.8	65.4	74.1	0.82

<sup>a</sup> Reaction conditions: Catalyst weight, 0.5 g; T, 240 °C; P, 1.0 MPa; H<sub>2</sub>/CO, 2; W<sub>Catalyst</sub>/F, 10 gh/mol; <sup>b</sup> C<sub>iso</sub>/C<sub>n</sub> is the ratio of isoparaffin to paraffin of C<sub>4+</sub>.

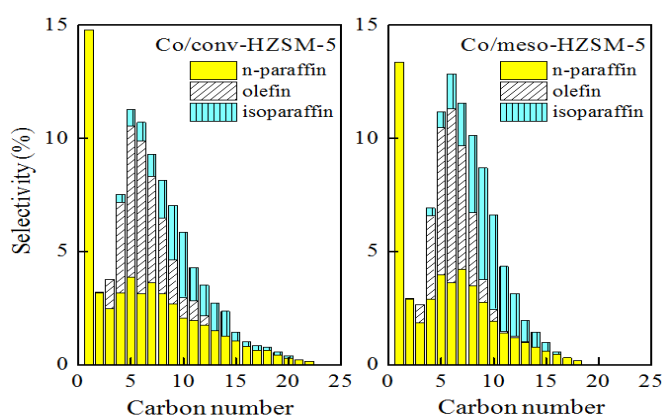


**Fig.9** FTS product distribution of Co/Conv-HZSM-5 and Co/meso-HZSM-5 catalysts.

#### 4. 結論・考察 (Conclusions)

CO<sub>2</sub> methanation was enhanced by preparing nanoparticles promoted bimodal pore catalysts. Moreover, ZrO<sub>2</sub> and Al<sub>2</sub>O<sub>3</sub> nanoparticles promoted catalysts exhibited high CH<sub>4</sub> selectivity and stability owing to their high capability for CO<sub>2</sub> chemisorption and activation, as well as strong interaction with nickel. Due to the excellent activity, selectivity and stability, ZrO<sub>2</sub> nanoparticles modified Ni-based bimodal catalyst exhibited high potential for the application in CO<sub>2</sub> methanation in the future. Furthermore, an optimal route for synthetic oil production was achieved by designing the catalysts with the hierarchical structure. The sputtered catalyst exhibited much higher CO conversion and isoparaffins selectivity than the

catalyst prepared by conventional impregnation. The hierarchical HZSM-5 with micropore and mesopore structure supported Co catalyst was employed to catalyze FTS reaction for direct synthesis of isoparaffin, exhibiting higher CO conversion and C<sub>5+</sub> selectivity, compared with the conventional HZSM-5 supported Co catalyst. The methods for the redesigning structure of the catalysts will be meaningful in the field of synthetic oil production.

## References

- (1) X. Zhang, W.J. Sun and W. Xu, *J. Fuel Chem. Technol.*, 2013, 41, 96.
- (2) W. Wang and J. Gong, *Front Chem. Sci. Eng.*, 2011, 5, 2.
- (3) G. A. Du, S. Lim, Y. H. Yang, C. Wang, L. Pfefferle and G. L. Haller, *J. Catal.*, 2007, 249, 370.
- (4) R. Phienluphon, L. Shi, J. Sun, W. Q. Niu, P. Lu, P. F. Zhu, T. Vitidsant, Y. Yoneyama, Q. J. Chen and N. Tsubaki, *Catal Sci Technol*, 2014, 4, 3099.
- (5) J. Sun, G. H. Yang, Q. X. Ma, I. Ooki, A. Taguchi, T. Abe, Q. Xie, Y. Yoneyama and N. Tsubaki, *J Mater Chem A*, 2014, 2, 8637.
- (6) V. A. de la Pena O'Shea, M. Consuelo Alvarez Galvan, A. E. Platero Prats, J. M. Campos-Martin and J. L. G. Fierro, *Chem Commun*, 2011, 47, 7131.